

Efficient method for determination of methylene blue dye in water samples based on a combined dispersive solid phase and cloud point extraction using $\text{Cu}(\text{OH})_2$ nanoflakes: central composite design optimization

Farzin Nekouei¹ · Hanieh Kargarzadeh² · Shahram Nekouei¹ · Farzaneh Keshtpour³ · Abdel Salam Hamdy Makhlouf⁴

Received: 10 August 2016 / Revised: 27 September 2016 / Accepted: 10 October 2016 / Published online: 4 November 2016
© Springer-Verlag Berlin Heidelberg 2016

Abstract A new method was developed for the efficient spectrophotometric determination of methylene blue (MB) dye in solutions. The method is based on a combined dispersive solid phase and cloud point extraction using $\text{Cu}(\text{OH})_2$ nanoflakes (as an adsorbent). $\text{Cu}(\text{OH})_2$ nanoflakes were synthesized by facile and fast methods and characterized using various techniques. The developed method is based on the adsorption of MB on the $\text{Cu}(\text{OH})_2$ nanoflakes and transfer into a surfactant-rich phase using Triton X-114 as a nonionic surfactant. Subsequently, MB dye is desorbed from $\text{Cu}(\text{OH})_2$ nanoflakes using a mixture of nitric acid and methanol solution and determined by UV–Vis spectrophotometry. The effects of pH, amount of $\text{Cu}(\text{OH})_2$ nanoflakes, volume (concentration of Triton X-114), and temperature were investigated by designing experiments using response surface methodology

(RSM). A quadratic model was utilized to predict the variables. Analysis of variance (ANOVA) was applied for the analysis of variables and their interactions, and optimal conditions were established. The results demonstrated logical agreement between experimental and predicted values of the response owing to high F value, low P value, and low lack-of-fit. The calibration graph was linear in the range of 2.0–350.0 $\mu\text{g L}^{-1}$ of MB dye with a correlation coefficient (R) of 0.9996. The limits of detection and quantification were found to be 0.65 and 2.05 $\mu\text{g L}^{-1}$, respectively. The developed method was successfully applied to different water samples, thereby confirming the applicability of the approach.

Keywords Methylene blue dye · $\text{Cu}(\text{OH})_2$ nanoflakes · Combined dispersive solid phase and cloud point extraction · Response surface methodology · Central composite design

Electronic supplementary material The online version of this article (doi:10.1007/s00216-016-0026-7) contains supplementary material, which is available to authorized users.

✉ Farzin Nekouei
f.nekouei@hotmail.com; fa.nekouei@gmail.com

- ¹ Young Researchers and Elites Club, Science and Research Branch, Islamic Azad University, Tehran, Iran
- ² Faculty of Science and Technology, School of Chemical Sciences and Food Technology, Polymer Research Center (PORCE), Universiti Kebangsaan Malaysia (UKM), 43600 Bangi, Selangor, Malaysia
- ³ Young Researchers and Elite Club, Central Tehran Branch, Islamic Azad University, Tehran, Iran
- ⁴ Manufacturing and Industrial Engineering Department, College of Engineering and Computer Science, University of Texas Rio Grande Valley, 1201 West University Drive, Edinburg, TX 78541-2999, USA

Introduction

Every year, millions of tons of colored wastewater are discharged from various sources such as textile, plastic, cosmetics, printing, leather, paper-making, and dye manufacturing industries [1–3]. It is essential to treat the colored synthetic compounds as they are often harmful to humans and the environment [1]. Dyes are one of the most abundant pollutants that in aquatic systems they can cause various problems such as reduced light penetration, carcinogenic and mutagenic changes, and increase in chemical oxygen demand (COD) and biochemical oxygen demand (BOD) of water systems that reflect its low quality [4]. Methylene blue [3,7-bis(dimethylamino)phenothiazin-5-ium chloride], a thiazine cationic dye (Table S1, see Electronic Supplementary Material, ESM), causes injury to human and animal eyes and skin [5–7]. Conventional and most applicable protocols for removal of dyes

from wastewaters include adsorption [8–13], flocculation [14], membrane filtration [15], electrolysis [16], biological treatments [17], and oxidation [18]. Among these, adsorption of dye molecules onto a substrate (adsorbent) is considered a simple, efficient, and cost-effective method for wastewater treatment [19]. Nanoparticle-based adsorbents possess high surface area along with various non-saturated reactive surface atoms that allow for selective and reversible binding of dye molecules [4, 20, 21].

Cloud point extraction (CPE) methodology is simple, cheap, highly efficient, and low-toxicity method compared to the conventional extraction systems [22–28]. CPE is based on the phase behavior of nonionic surfactants in aqueous solutions, which exhibit phase separation after an increase in temperature or the addition of a chelating agent [29]. As the CPE is primarily based on the hydrophobic interaction between the solutes and surfactant, other hydrophobic species can be extracted into the surfactant rich-phase and may interfere with the analysis of the analytes of interest [30].

Surface enhance methodology (RSM) is a collection of statistical and mathematical methods that are useful for modeling and analyzing engineering problems [31]. The main objective of RSM is to optimize the response surface that is influenced by various process parameters. RSM also quantifies the relationship between the controllable input parameters and the obtained response surfaces [31, 32].

To the best of our knowledge, there are only a few published articles regarding combined CPE and solid phase extraction (SPE) [33–36], and only one of those [33] developed a new synthesized adsorbent. In this work, we first synthesized $\text{Cu}(\text{OH})_2$ nanoflakes using a simple, fast, and low-cost method. We then applied the synthesized $\text{Cu}(\text{OH})_2$ nanoflakes as solid nanosubstrates for adsorption of methylene blue dye (MB) and for carrying out the CPE procedure for preconcentration/separation of $\text{Cu}(\text{OH})_2$ -nanoflakes-MB from aqueous solutions in a micellar medium. After separating the $\text{Cu}(\text{OH})_2$ -nanoflakes-MB from the micellar medium by centrifugation and eluting using a suitable eluant, we measured the resulting absorbance by UV-vis spectrophotometry. Finally, we used RSM and central composite design (CCD) to model the influence of some operating parameters on the performance of the MB extraction.

Experimental

Materials and chemicals

All chemicals used were analytical grade and solutions were prepared with distilled water. Triton X-114 was purchased from prepared Sigma-Aldrich, Steinheim, Germany. All the other chemicals used were purchased from Merck, Darmstadt, Germany.

Materials characterization

X-ray diffraction (XRD)

XRD measurements were conducted using a Bruker AXS-D8 Advance model system. The diffracted intensity of the $\text{Cu K}\alpha$ radiation (0.154 nm, 40 kV, and 40 mA) was measured over a 2θ range between 5.0 and 80.

Field emission scanning electron microscopy (FESEM)

FESEM was performed on a Zeiss Supra, model 55VP, Germany.

Fourier transform infrared spectroscopy (FTIR)

A PerkinElmer FTIR spectrophotometer equipped with an attenuated total reflectance accessory configured with a KSR-5 crystal (ATR) was used to record IR spectra in the region $4000\text{--}400\text{ cm}^{-1}$.

Dynamic light scattering

The particle size and size distribution of the $\text{Cu}(\text{OH})_2$ nanoflakes were measured by dynamic light scattering using a Zetasizer Nanoseries system (Malvern Instruments Co., Malvern, UK). The material absorption unit was 0.001 w/v %.

UV-Vis spectroscopy

A double beam spectrophotometer (UV-1800, Shimadzu, Japan) was used to determine the concentration of MB at 675 nm.

Surface area analysis

The surface area and pore size distribution of the sorbent were determined from the corresponding nitrogen adsorption-desorption isotherms at 77 K using a Micromeritics ASAP 2020 system. The surface area was determined by the Brunauer-Emmett-Teller (BET), Langmuir, and Barrett-Joyner-Halendathe (BJH) equations, and pore size distribution was calculated by using the BET and BJH equations.

Preparation of $\text{Cu}(\text{OH})_2$ nanoflakes

$\text{Cu}(\text{OH})_2$ nanoflakes were synthesized by a precipitation method using CuCl as the initial chemical reagent and ammonium as the precipitation agent. First, 0.5 g of CuCl was dissolved in 35 mL NH_3 (2.0 M) in a 100-mL flask. Next, 1 mL of tetrahydrofuran (THF) and 0.5 mL oleic acid (as surfactant) were added, and the mixture was stirred strongly at 80 °C ($\text{pH} \leq 10$) using a magnetic

stirrer. The dark blue suspension remained under constant and strong stirring for 120 min. Subsequently, the suspension was filtered and washed several times with a mixture of distilled water and ethanol to remove impurities. Finally, the obtained precipitate was dried at ambient temperature in a vacuum oven at 0.1 MPa for 7 h before characterization.

Analytical methods

A 0.0055 g portion of $\text{Cu}(\text{OH})_2$ nanoflakes was added to 3 mL of 3 % (v/v) of Triton X-114. In order to completely disperse the $\text{Cu}(\text{OH})_2$ nanoflakes, the mixture of nanoparticles and nonionic surfactant was stirred for 2 min. Then, the following reagents were added to the above mixture: an aliquot of MB solution, 2 mL of phthalate buffer solution, and 1 mL of Na_2SO_4 (1 M), (50 mL final solution). The mixture was placed in a water bath at 45 °C for 20 min to allow phase separation. Then, the flask was put in an ice bath for 5 min, so the supernatant (aqueous phase) was easily decanted. Subsequent centrifugation at 4000 rpm for 5 min allowed the $\text{Cu}(\text{OH})_2$ nanoflakes to be separated from the surfactant rich-phase medium. In order to wash the nanoflakes and separate the MB adsorbed onto nanoflakes, 500 μL of a mixture of HNO_3 (1 M) and methanol (1:1 ratio) was added to $\text{Cu}(\text{OH})_2$ nanoflakes and centrifuged for 2.5 min. Finally, the supernatant solution (eluate) was collected in a 700 μL cuvette and its absorbance was determined by UV–Vis spectrophotometer at 675 nm. The blank solution was prepared using the same procedures but in the absence of MB.

Samples preparation

The developed method was applied to different samples including domestic wastewater, water from Karoon river (located in an industrial city, Ahvaz), and water from Beshaar river (Yasouj city). All samples were filtered through a 0.22 μm membrane to remove the suspended and floating particles.

Experimental design

RSM was used for the modeling and analysis of the effects of experimental variables in order to optimize them [37]. A CCD was used to determine the optimal conditions for the critical factors [38]. For the CPE/SPE process, effective variables such as pH, $\text{Cu}(\text{OH})_2$ nanoflakes dose, the volume of 3 % Triton X-114 (v/v), and temperature were chosen as independent variables and designated as X_1 – X_4 , respectively. As shown in Table 1, the pH (X_1) ranged from 4 to 8, $\text{Cu}(\text{OH})_2$ nanoflakes dose (X_2) ranged from 0.001 to 0.01 g, Triton X-114 volume (X_3) ranged from 1.0 to

Table 1 Design matrix for the central composite designs

Factors	Levels				
	Low (−1)	Central (0)	High (+1)	− α	+ α
X_1 : pH	5	6	7	4	8
X_2 : adsorbent dose (g)	0.00325	0.00550	0.00775	0.001	0.01
X_3 : TX-114 volume (mL)	2	3	4	1	5
X_4 : temperature (°C)	35	45	55	25	65

5.0 mL of 3 % (v/v), and the temperature (X_4) ranged from 25 to 65 °C. According to Eq. (1), setting the lowest values as -2 and the highest values as $+2$, the real values of the independent variables (X_i) were coded as Z_i [39]:

$$Z_i = \frac{X_i - X_0}{\Delta X_i} \quad (1)$$

where z_i is the dimensionless value of an independent variables, x_i represents the real value of the independent variable, x_0 is the real value of the independent variable at the center point, and Δx_i is the step change [39, 40]. According to Eq. (2), the total number of experimental points needed (N) is determined [37]:

$$N = 2^k + 2k + C_0 \quad (2)$$

Therefore, a total of 30 experiments ($k = 4$, $C_0 = 6$) were performed. The following second-order polynomial equation was used to analyze the experimental results:

$$Y = \beta_0 + \sum_{i=1}^n \beta_i X_i + \sum_{i=1}^n \beta_{ii} X_i^2 + \sum_{i < j=1}^n \beta_{ij} X_i X_j + \varepsilon \quad (3)$$

where Y is the predicted response, β_0 is the coefficient for intercept, β_i is the coefficient of linear effect, β_{ii} is the coefficient of quadratic effect, β_{ij} is the coefficient of interaction effect, ε is the term that represents other sources of variability not accounted for by the response function, and X_i and X_j are coded independent variables (Table 2).

Analysis of variance (ANOVA) as the most powerful numerical method for model validation was performed to estimate the different causes of variation. ANOVA can determine to what extent altering a controlled factor leads to a significant difference between the mean values obtained [37]. Also, it checks the adequacy of the regression model (R^2) in terms of lack-of-fit test, i.e., non-modeled variation in response [37]. The validated model can be plotted as a three-dimensional graph to generate a surface response corresponding to a response function that allows one to determine the best operating conditions. The significance of each process variable was checked by p value and F value.

Table 2 Experimental design matrix for the CCD

Run	X_1	X_2	X_3	X_4	MB absorbance		Residual
					Observed ^a	Predicted ^b	
1	6.0	0.00775	3.0	45.0	1.100	1.067	-1.100
2	5.0	0.00100	4.0	35.0	0.600	0.625	-0.608
3	7.0	0.00550	2.0	55.0	0.700	0.742	-1.014
4	6.0	0.00550	3.0	45.0	1.100	1.067	0.550
5	7.0	0.00325	4.0	55.0	1.500	1.492	0.203
6	6.0	0.00325	3.0	45.0	0.700	0.671	0.710
7	6.0	0.00550	3.0	45.0	1.000	1.067	-1.147
8	6.0	0.00775	10	45.0	0.700	0.621	1.926
9	5.0	0.00775	2.0	55.0	0.400	0.396	0.101
10	5.0	0.00325	4.0	55.0	0.800	0.854	-2.027
11	6.0	0.00775	3.0	45.0	1.000	1.067	-1.147
12	5.0	0.00550	4.0	55.0	0.800	0.796	2.449
13	5.0	0.00775	2.0	55.0	0.600	0.633	-0.811
14	7.0	0.00775	4.0	55.0	1.000	0.979	0.507
15	7.0	0.00325	2.0	55.0	1.350	1.429	-1.926
16	4.0	0.00325	3.0	45.0	0.300	0.263	0.912
17	7.0	0.00550	4.0	35.0	1.200	1.196	0.101
18	5.0	0.00775	2.0	35.0	0.550	0.563	-0.304
19	7.0	0.01000	4.0	35.0	0.800	0.833	-0.811
20	5.0	0.00550	2.0	35.0	0.400	0.475	-1.824
21	8.0	0.00325	3.0	45.0	1.200	1.179	0.507
22	7.0	0.00550	2.0	35.0	1.250	1.233	0.405
23	6.0	0.00550	3.0	45.0	1.300	1.271	0.710
24	6.0	0.00550	3.0	45.0	1.100	1.067	0.550
25	7.0	0.00325	2.0	35.0	0.700	0.696	0.101
26	6.0	0.00550	5.0	45.0	1.300	1.345	-0.507
27	6.0	0.00550	3.0	65.0	1.100	1.029	1.723
28	6.0	0.00550	3.0	45.0	1.100	1.067	0.573
29	5.0	0.00325	4.0	35.0	0.800	0.713	2.129
30	6.0	0.00550	5.0	25.0	0.600	0.695	-0.304

^a Experimental of values of response^b Predicted values of response by RSM presented method

Results and discussion

Characterization of Cu(OH)₂ nanoflakes

Optical absorption

The measurement of the band gap of materials is important in semiconductor, nanomaterial, and solar industries. From the absorption spectrum (Fig. S1, see ESM), band gap energy of Cu(OH)₂ nanoflakes was obtained using the following relation [41]:

$$(\alpha h\nu)^2 = A(h\nu - E_g) \quad (4)$$

where E_g is the band gap energy, A is a constant related to the material and matrix element of the transition, ν is the frequency of the incident radiation, h is Planck's constant, α is the absorption coefficient in reciprocal centimeters (cm^{-1}) [42]. The band gap energy was determined by plotting $(\alpha h)^2$ versus energy ($h\nu$) and extrapolating the linear portion of the respective curve to $(\alpha h)^2 = 0$ [43]. According to ESM Fig. S1, the absorption edge of Cu(OH)₂ nanoflakes (ca. 282 nm) is 4.4 eV, which agrees with the reported values for Cu(OH)₂ [44].

FESEM

Figures S2a and S2b (see ESM) show images of the Cu(OH)₂ nanoflakes at different magnifications. From ESM Fig. S2a, it can be seen that the sample contains plenty of flake-like morphology. Interestingly, the Cu(OH)₂ nanoflakes possess a huge porous surface with numerous boundaries that can improve the adsorption efficiency of MB dye. ESM Fig. 2Sb reveals that each "flake" comprises a large number of nano-sheets, which look like "flakes". The nanoflakes have an average thickness of less than 50 nm. The flake structures are approximately regular and uniform and exhibit almost the same shape and size in Fig. 2Sb (ESM).

XRD

The XRD pattern of the flower-like Cu(OH)₂ nanoflakes is presented in Fig. S3 (see ESM). According to the reference (JCPDS card no. 00-035-0505), the nanoflakes have an orthorhombic crystal system and a 63 space group number. The peaks around 16.73°, 23.76°, 33.95°, 35.88, 38.06°, 39.78°, and 53.28° reveal tetragonal structure and are assigned to the (020), (021), (002), (111), (041), (130), and (150) crystalline planes of the Cu(OH)₂ nanostructure, respectively. No diffracted peaks due to impurities were observed. The mean crystal size was calculated using the Debye–Scherrer formula represented in Eq. (5) [9]:

$$D = 0.9\lambda / \beta \cos\theta \quad (5)$$

From the equation, the mean crystal size of nanoflakes was ascertained to be 32.818 nm, which is in agreement with the FESEM image (ESM Fig. 2Sc). The obtained mean crystal size is comparable with previous works reported in the literature [44, 45].

Dynamic light scattering

Dynamic light scattering (DLS) is the most suitable technique for estimation of the sizes of nanoparticles dispersed or dissolved in solvents [46]. DLS histograms of Cu(OH)₂ nanoflakes are given in Fig. S4 (see ESM). The

average hydrodynamic diameter for Cu(OH)₂ nanoflakes was less than 400 nm with a size distribution of 0.389 polydispersity (ESM Fig. S4).

Surface area analysis

The BET method was utilized to further analyze the surface area properties and nitrogen adsorption–desorption isotherm (Fig. S5, see ESM). According to Fig. S5, the isotherm is convex naturally up to $P/P_0 = 1$, and the corresponding pore size distributions reveal the mesoporous nature of the sample. The BET surface area of Cu(OH)₂ nanoflakes was calculated to be 16.6 m² g⁻¹ with respective pore volumes of 0.019 cm³ g⁻¹ nm⁻¹. The calculated surface area is better or comparable to the previous studies [47].

FTIR characterization

The FTIR spectrum in Fig. S6 (see ESM) provides information about interactions between the Cu(OH)₂ nanoflakes. The IR bands at 3443 and 1618 cm⁻¹ are assigned to the stretching vibrations of OH groups and physically adsorbed H₂O, respectively [47, 48]. The bands at 1025 and 888 cm⁻¹ correspond to the C–O stretching vibration (probably related to trace amount of oleic acid used as a precursor) coordinating to metal cations (Cu²⁺) in Cu(OH)₂ [47–50]. The medium band at 435 cm⁻¹ is assigned to the Cu–O stretching mode [48, 51].

Central composite design (CCD)

Model fitting and statistical analysis

Four independent variables were selected in this study to evaluate the influence of operating parameters on the removal efficiency of MB dye. As shown in Table 1, the variables are pH (X_1) in the range 4–8, Cu(OH)₂ nanoflakes dose (X_2) in the range 0.001–0.01 g, Triton X-114 volume (X_3) in the range 1–5 mL of 3 % (v/v), and temperature (X_4) in the range 25–65 °C. The variables were assigned one of three levels (low, basal, and high) with coded value (–1, 0, +1) and their star points of +2 and –2 for + α and – α respectively were selected for each set of experiments. A total of 30 experiments this work were used for the response surface modelling. ANOVA was also used to identify significant factors. Table 3 presents ANOVA results for MB removal by combined solid phase–cloud point extraction using the dispersion of Cu(OH)₂ nanoflakes. ANOVA was applied to examine the fitness and accuracy of the model, effects of single variables, and interaction effects on the response [52]. The larger the magnitude of F value and, correspondingly, the smaller the “Prob. > F ” value is, the more significant the corresponding coefficient [53]. The model F value is 46.08 with lower probability (<0.0001) indicating that the model is significant.

Table 3 Analysis of variance for central composite design for MB dye analysis

Source of variation	Sum of squares	Df	Mean square	F value	P value	
Model	2.62	14	0.19	46.08	<0.0001	#
X_1	1.26	1	1.26	310.79	<0.0001	#
X_2	0.54	1	0.54	133.15	<0.0001	#
X_3	0.13	1	0.13	33.29	<0.0001	#
X_4	0.070	1	0.070	17.36	0.0008	#
X_1X_2	0.20	1	0.20	49.93	<0.0001	#
X_1X_3	1.00E–02	1	1.00E–02	2.47	0.1372	*
X_1X_4	0.016	1	0.016	3.85	0.0685	*
X_2X_3	0.031	1	0.031	7.55	0.0149	#
X_2X_4	0.022	1	0.022	5.55	0.0325	#
X_3X_4	1.00E–02	1	1.00E–02	2.47	0.1372	*
X_1^2	0.21	1	0.21	50.56	<0.0001	#
X_2^2	0.016	1	0.016	3.88	0.0676	*
X_3^2	0.15	1	0.15	36.99	<0.0001	#
X_4^2	0.036	1	0.036	8.99	0.0090	#
Residual	0.061	15	4.056E–03	–	–	
Lack-of-fit	0.047	10	4.75E–03	1.78	0.2721	*
Pure error	0.013	5	2.67E–03	–	–	
Cor Total	2.68	29	–	–	–	

Df degree of freedom, # significant, * not significant
 $R^2 = 0.9773$; Adj- $R^2 = 0.9561$; Pred- $R^2 = 0.8906$

There was only a 0.01 % possibility that the model F value could happen due to noise. As can be seen in Table 3, among the four variables studied, pH (X_1) has the largest effect on the removal of MB owing to the maximum F value followed in order by adsorbent dose (X_2), Triton X-114 volume (X_3), and temperature (X_4). The lack-of-fit for F value of 1.78 ($p = 0.2721$) indicates that this term is not significant to the pure error. The “Pred- R^2 ” of 0.8906 is in reasonable agreement with the “Adj- R^2 ” of 0.9561. Based on data analysis (Table 3), an empirical second-order polynomial equation was obtained, which in terms of coded factors is as follows:

$$y_{\text{Abs}} = +1.07 + 0.23X_1 + 0.15X_2 + 0.075X_3 + 0.054X_4 + 0.11X_1X_2 - 0.044X_2X_3 + 0.037X_2X_4 - 0.086X_1^2 - 0.074X_3^2 - 0.036X_4^2 \quad (6)$$

where y is absorption of MB and X_1 , X_2 , X_3 , and X_4 are the variables as mentioned above and presented in Table 1. In addition, the final equation in terms of actual factors is as follows:

$$y_{\text{Abs}} = -3.330 + 0.926X_1 - 197.942X_2 + 0.6634X_3 + 2.813E-003X_4 + 50.000X_1X_2 - 19.444X_2X_3 + 1.666X_2X_4 - 0.0864X_1^2 - 0.0740X_3^2 - 3.646E-004X_4^2 \quad (7)$$

Table 4 Estimated regression coefficients

Factor	Coefficient	Std. err.	<i>t</i> value	<i>p</i> value
Intercept	1.07	0.026	1.22	0.0000
X_1	0.23	0.013	0.26	0.0000
X_2	0.12	0.014	0.15	0.0000
X_3	0.075	0.013	0.10	0.0000
X_4	0.054	0.013	0.082	0.0008
X_1X_2	0.110	0.016	0.150	0.0000
X_1X_3	-0.025	0.016	0.0089	0.1372
X_1X_4	0.031	0.016	0.065	0.0685
X_2X_3	-0.044	0.016	-0.0098	0.0149
X_2X_4	0.037	0.016	0.071	0.0325
X_3X_4	0.025	0.016	0.059	0.1372
X_1^2	-0.086	0.012	-0.061	0.0000
X_2^2	-0.024	0.012	0.00196	0.0676
X_3^2	-0.074	0.012	-0.048	0.0000
X_4^2	-0.036	0.012	-0.011	0.0090

The estimated regression coefficients, *t* values, and *P* values are given in Table 4. The significance of each model term was checked using *P* values. *P* values smaller than 0.05 indicate that the model is statistically significant, while values greater than 0.1000 indicate the model terms are not significant [52]. In this case all the linear model terms (X_1 , X_2 , X_3 , and X_4), the three quadratic model terms (X_1^2 , X_3^2 , and X_4^2), and the one interaction term (X_1X_2 , X_2X_2 , X_2X_4) are significant. The rest do not have a

significant effect on the adsorption of MB because the *p* value is more than 0.05 (X_1X_3 , X_1X_4 , X_3X_4 , and X_2^2).

Figure 1a shows the comparison of predicted and experimental absorption of MB dye. The nearness of the points to the diagonal line indicates the good fit of the model, because the value of predicted R^2 of 0.8906 is in good agreement with the adjusted R^2 of 0.9561. Figure 1b shows the relationship between the normal probability (%) and the internally studentized residuals, and the high linearity shows that neither response transformation was required nor was there an apparent problem with normality [52, 54]. Adequate precision measures the signal to noise ratio. A ratio greater than 4 is desirable. Interestingly, our result is 27.296 indicating an adequate signal. Therefore, this model can be successfully used to navigate the design space.

Response surface methodology analysis

In order to gain a better understanding of the interaction effects of variables on recovery as well as the relationship between the variables and responses, three-dimensional (3D) and two-dimensional (2D) plots were drawn. The nature and extent of the effects of the interactions between the experimental factors on the response are understandable from the shape of the contour plot [55]. In fact, when the shape of contour plot is circular, it shows negligible interaction between the equivalent variables. On the other hand, an elliptical or saddle-

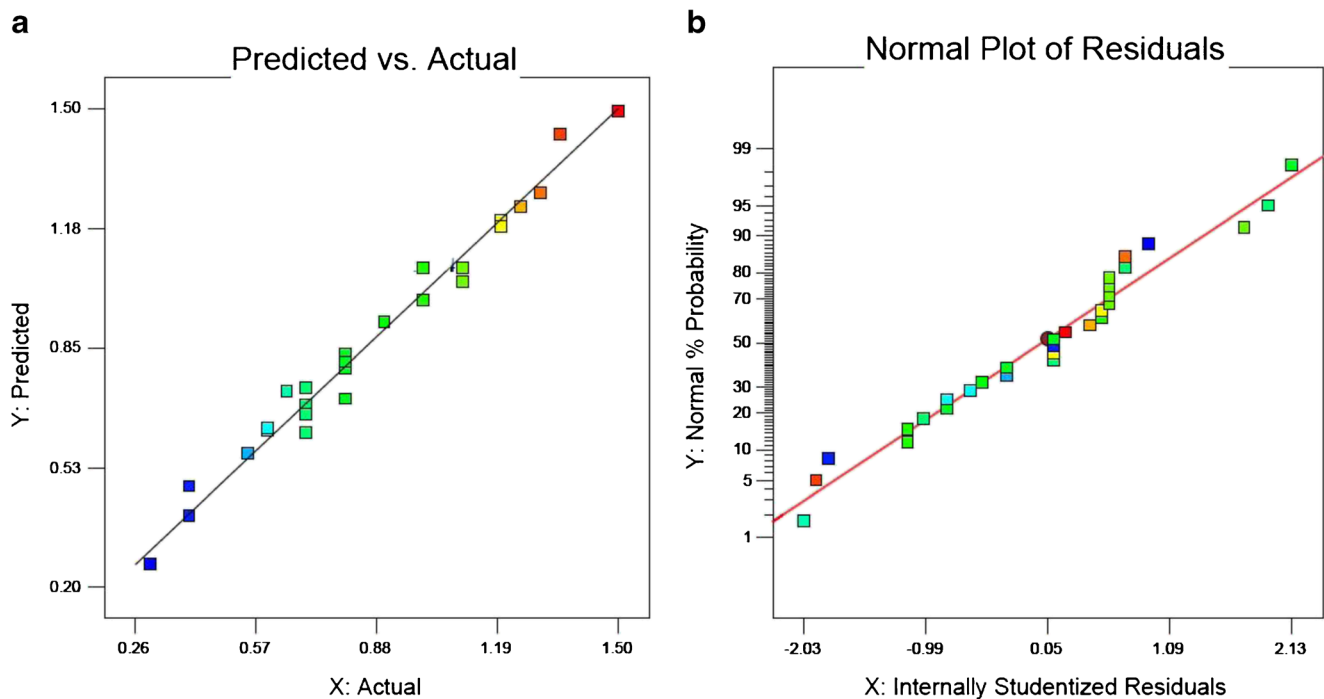


Fig. 1 a Comparison of predicted and experimental absorption MB dye. b Relationship between the normal probability (%) and the internally studentized residuals

type contour plot indicates significant interaction between the equivalent variables [56].

As mentioned above, the roles of pH and adsorbent dose are considered to be the most influencing variables in the absorption process. Figure 2 describes the effect of the combination of pH and adsorbent dose at constant values of temperature and Triton X-114 volume (concentration). The absorption efficiency of MB dye increases with increasing the pH just above 7 because of increasing the OH^- concentration on the surface of the adsorbent that preferably attracts positively charged ions like MB dye [9]. However, beyond this pH value the absorption efficiency starts to decrease which because at pH values higher than 7 the surface of the adsorbent gets highly negative charged because OH^- ions can occupy the free sites on the adsorbent. At pHs lower than 7, the surface of the adsorbent has positive charge due to protonation of functional groups of $\text{Cu}(\text{OH})_2$ in highly acidic solution which

disfavors the adsorption of cationic ions like MB [9]. The amount of adsorbent is another important parameter to control the capacity of the adsorbent. On the basis of Fig. 8, the adsorption efficiency remarkably increases with increasing the amount of adsorbent at constant pH value as a result of increasing the available surface area for adsorption. After that, it does not affect the absorption efficiency.

At constant pH value (pH 7), the MB absorption efficiency increases with increasing the Triton X-114 concentration (volume) (Fig. 3). At lower Triton X-114 concentrations, the extraction yield is slightly lower probably because of the inadequacy of assemblies to entrap the hydrophobic analyte quantitatively [57]. On the other hand, adding extra amounts of Triton X-114 above the optimum value causes a decrease in the extraction efficiency which leads to an increase in the viscosity of the surfactant-rich phase, which may increase the turbidity of the sample solutions especially the blank solution [57].

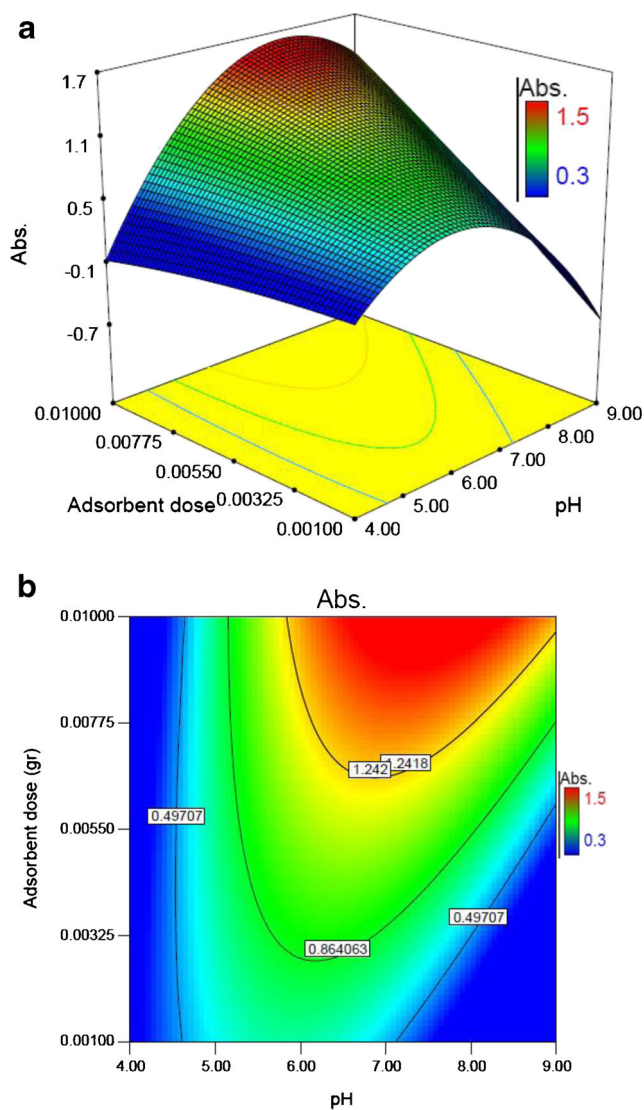


Fig. 2 Response surfaces for the MB extraction: **a** 3D surface X_1 - X_2 ; **b** 2D contour X_1 - X_2

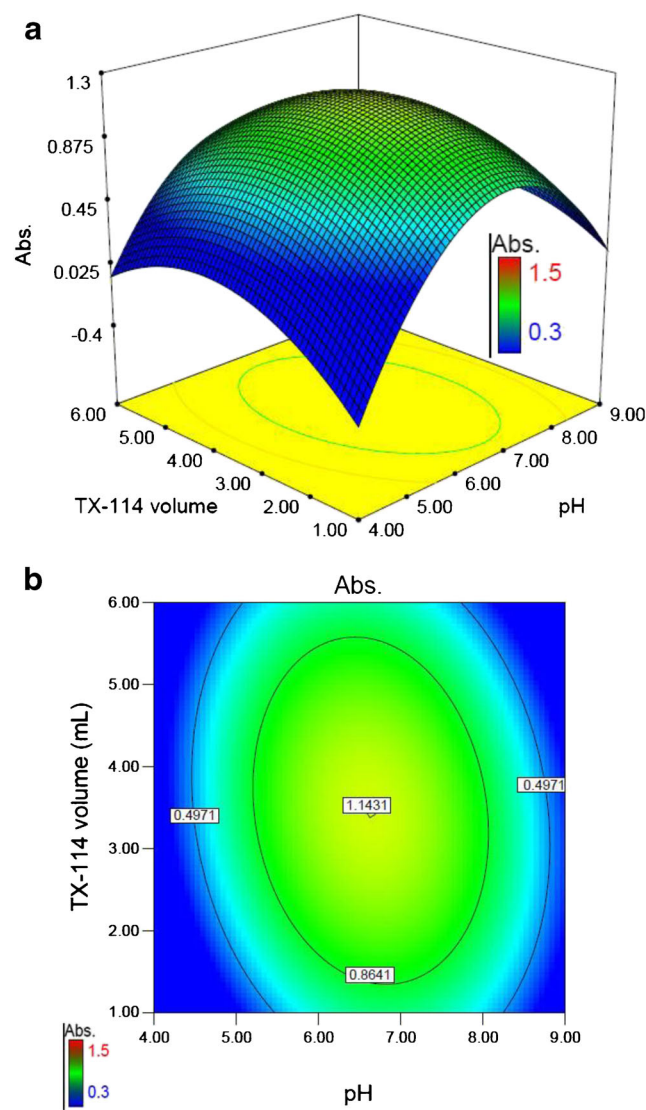


Fig. 3 Response surfaces for the MB extraction: **a** 3D surface X_1 - X_3 ; **b** 2D contour X_1 - X_3

The maximum extraction efficiency of analytes occurs when the CPE process is carried out at the equilibrium temperature higher than the cloud point temperature of the surfactant (Triton X-114) [58]. Figure 4 shows the combined influence of pH and temperature under constant adsorbent dose and initial dye concentration conditions. At constant pH value, the MB absorption efficiency increases from 25 °C to 45 °C. At temperatures below 45 °C, the extraction efficiency decreases. That decrease is likely due to the insufficient separation of the surfactant and the aqueous phases resulting from the incomplete dissolution of Triton X-114 at those temperatures [59]. However, at temperatures higher than 45 °C, there is no remarkable change in the extraction efficiency.

The combined effects of Triton X-114 volume and adsorbent dose at constant temperature (45 °C) and pH 7 are

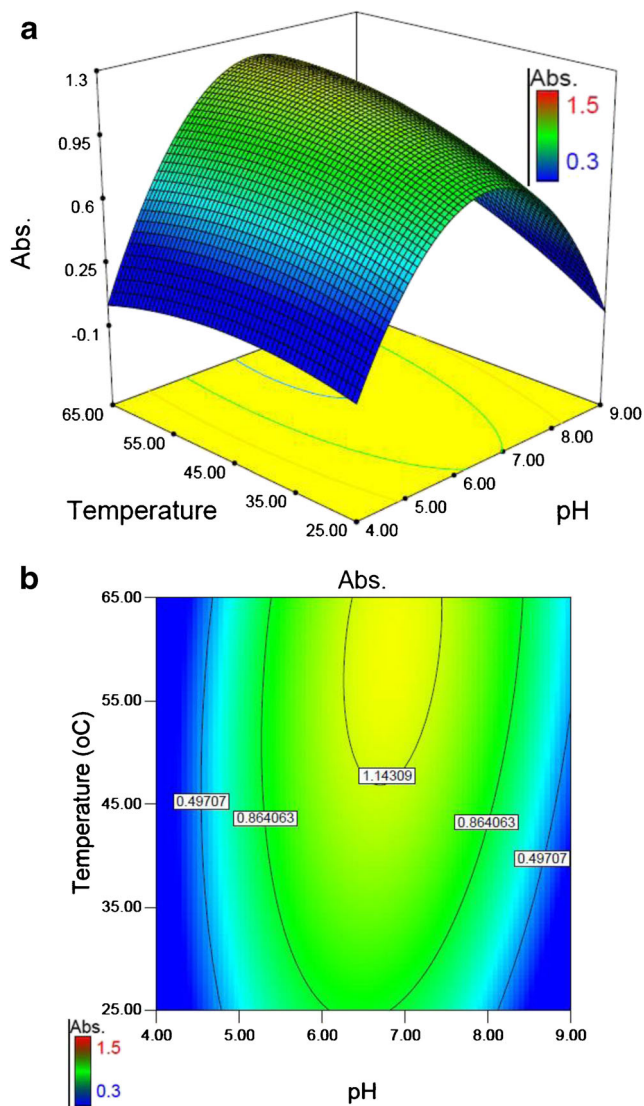


Fig. 4 Response surfaces for the MB extraction: **a** 3D surface X_1 – X_4 ; **b** 2D contour X_1 – X_4

given in Fig. 5. The increase of adsorbent dose is directly proportional to the increase in the extraction efficiency. Furthermore, at constant value of adsorbent dose, the extraction efficiency increases by increasing Triton X-114 concentration or volume up to 3 mL of 3 % (v/v) followed by a decrease thereafter.

Figure 6 shows the effect of both adsorbent dose and temperature on the extraction efficiency at constant pH 7 and Triton X-114 volume (3 mL of 3 % (v/v)). Increasing the temperature up to 45 °C at pH 7 increases the absorbance and becomes nearly constant thereafter.

Figure 7 displays the effect of the combination of Triton X-114 volume (concentration) and temperature at constant values of the pH 7 and adsorbent dose (0.0055 g). The extraction efficiency improves by increasing the temperature up to 45 °C and Triton X-114 concentration 3 mL of 3 % (v/v). A decline in absorbance value was observed by adding extra Triton X-114 volume after the optimum point.

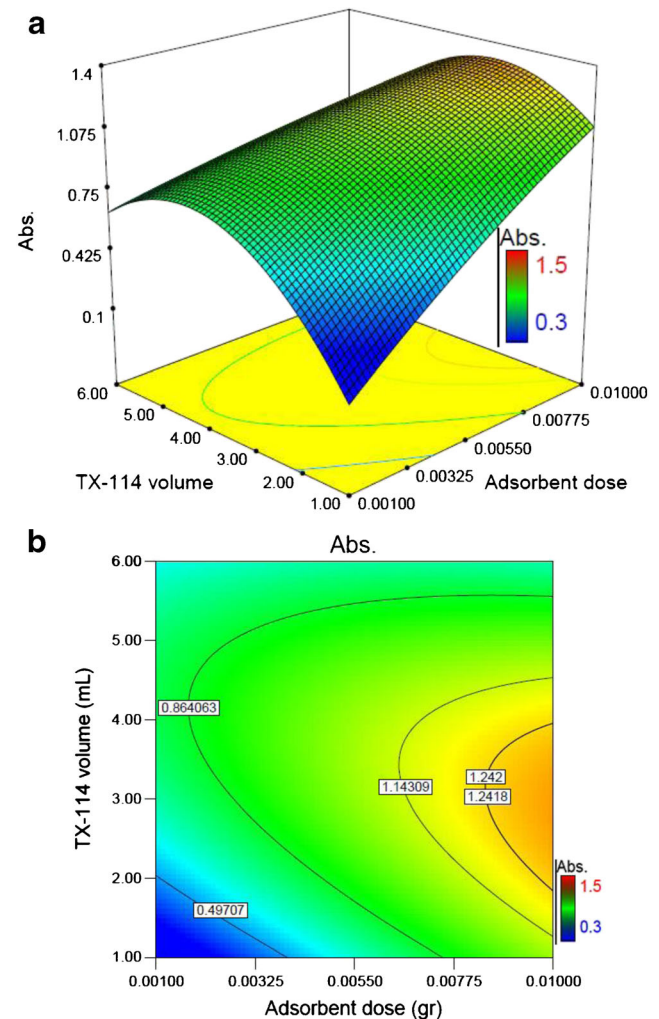


Fig. 5 Response surfaces for the MB extraction: **a** 3D surface X_2 – X_3 ; **b** 2D contour X_2 – X_3

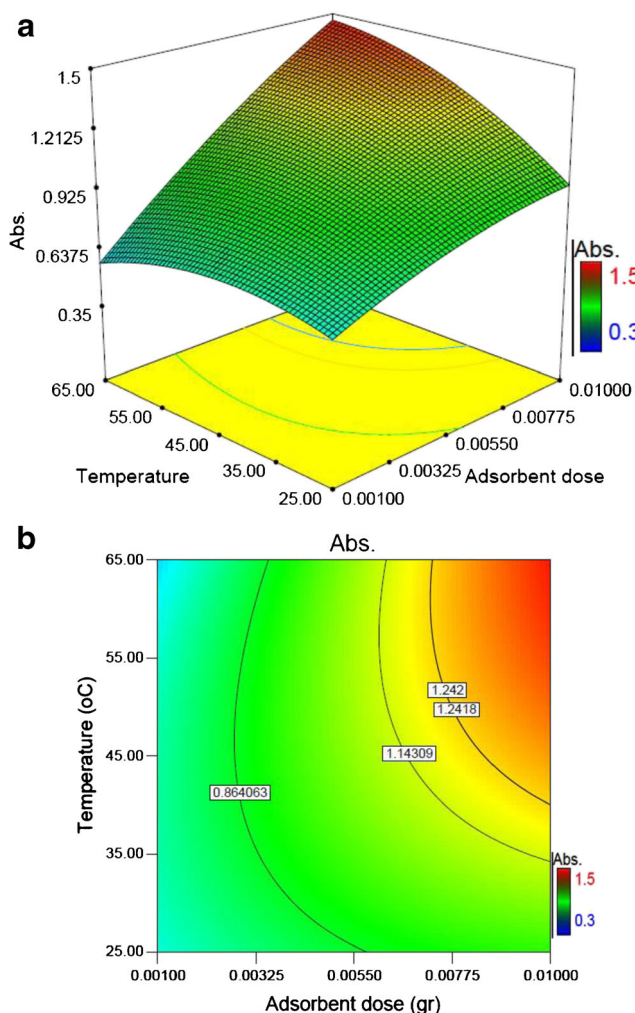


Fig. 6 Response surfaces for the MB extraction: **a** 3D surface X_2 – X_4 ; **b** 2D contour X_2 – X_4

Conformation of optimal conditions

The extraction efficiency and the operation conditions for maximum absorbance of MB dye from aqueous solution were calculated from the second-order equation obtained from the experimental data. The first-order partial differential equations obtained from Eq. (7) for X_i are

$$\frac{\partial Y}{\partial X_1} = +0.926 + 50.00X_2 - 0.0864X_1 \tag{8}$$

$$\frac{\partial Y}{\partial X_2} = -197.942 + 50.00X_1 - 19.444X_3 + 1.666X_4 \tag{9}$$

$$\frac{\partial Y}{\partial X_3} = +0.6634 - 19.444X_2 - 0.0740X_3 \tag{10}$$

$$\frac{\partial Y}{\partial X_4} = +2.813E-003 + 1.666X_2 - 3.646E-004X_4 \tag{11}$$

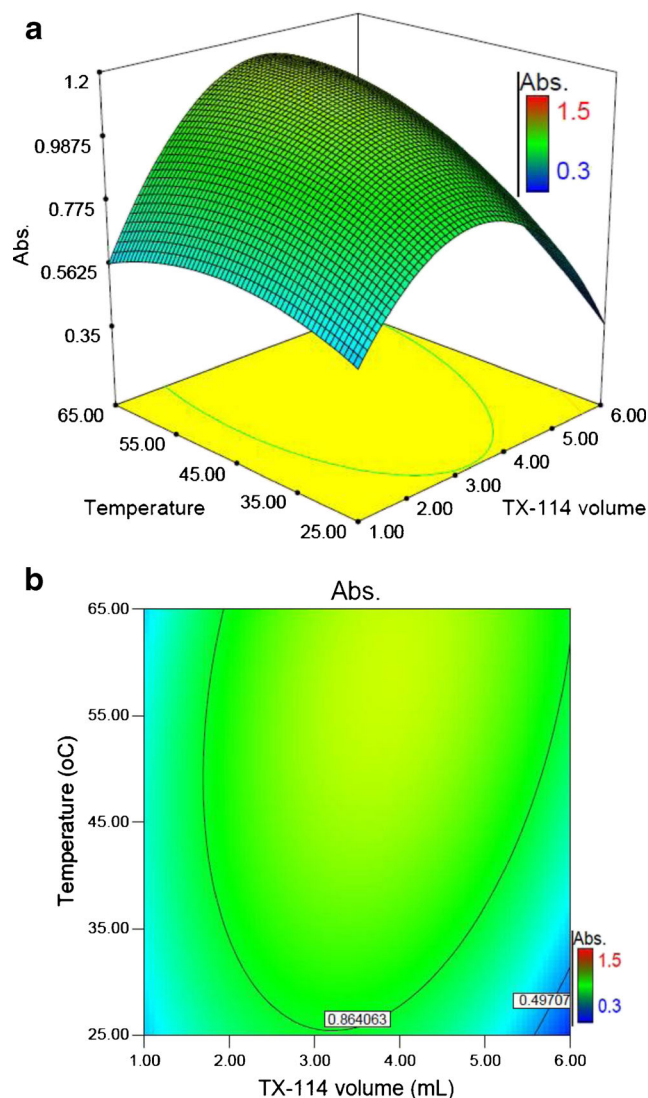


Fig. 7 Response surfaces for the MB extraction: **a** 3D surface X_3 – X_4 ; **b** 2D contour X_3 – X_4

The second-order differential equations are

$$\frac{\partial^2 Y}{\partial X_1^2} = -0.0864 \tag{12}$$

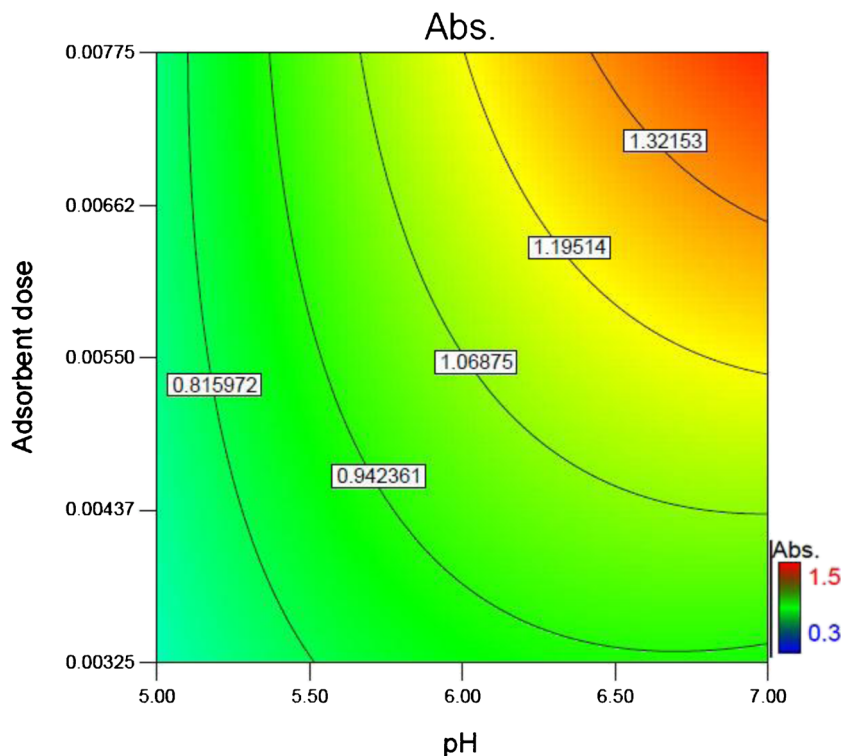
$$\frac{\partial^2 Y}{\partial X_2^2} = 00.00 \tag{13}$$

$$\frac{\partial^2 Y}{\partial X_3^2} = -0.0740 \tag{14}$$

$$\frac{\partial^2 Y}{\partial X_4^2} = -3.646E-004 \tag{15}$$

By considering $\frac{\partial Y}{\partial x_i} = 0$ resulting in maximum value of Y (absorbance) for Eqs. (8)–(11), the value of X_i (X_1 , X_2 , X_3 , and X_4) could be obtained. The solutions of Eqs. (8)–(11) were found to be $X_1 = 8.266$, $X_2 = -0.00424$, $X_3 = 10.078$, and

Fig. 8 Contour plot obtained from RSM optimization for optimum extraction efficiency



$X_4 = -11.643$. These values were then converted to actual values of X_1 (pH) = 7, X_2 (adsorbent dose) = 0.0055 g, X_3 (Triton X-114 concentration) = 3 mL of 3 % (v/v), and X_4 (temperature) = 45 °C (Table 1). Under the optimum conditions, the maximum predicted absorbance was 1.2094 with satisfactory desirability of 0.946 as shown in Fig. 8.

Adsorption capacity of Cu(OH)₂ nanoflakes

The adsorption capacity is an important parameter for the evaluation of an adsorbent, because it determines how much sorbent is required for the quantitative removal of an analyte in solution [60]. A batch method was adopted for the evaluation of the adsorption capacity of Cu(OH)₂ nanoflakes. The concentrations of MB were estimated using the linear regression equation obtained by plotting

its calibration curve. The removal percentage ($R\%$) was calculated using the following equation:

$$R\% = \left(\frac{C_0 - C_t}{C_0} \right) \times 100 \tag{16}$$

where C_0 (mg L⁻¹) and C_t (mg L⁻¹) are the initial concentration of dye and that after time t , respectively [8]. The dye adsorption capacities of the adsorbent were estimated for the two doses (0.0055 and 0.01 g) at room temperature, pH 7, and different initial MB dye concentration in a

Table 5 Langmuir isotherm constant and correlation coefficient calculated for the adsorption of MB onto the adsorbent

Isotherm	Parameters	Value of parameters	
		0.0055 g	0.010 g
Langmuir	Q_m (mg g ⁻¹)	122.68	88.72
	K_L (L mg ⁻¹)	1.10	1.56
	R^2	0.9965	0.9960

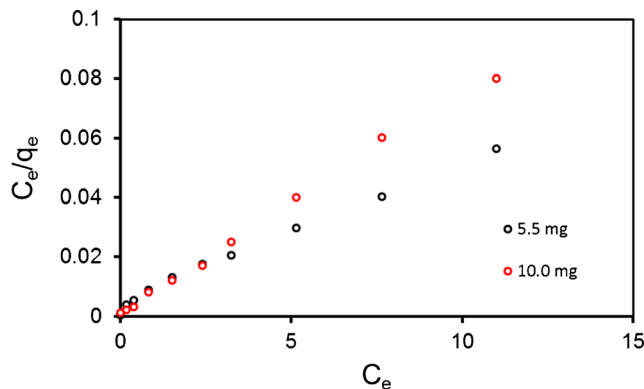


Fig. 9 Langmuir isotherm for the extraction of MB for 0.0055 and 0.010 g of Cu(OH)₂ nanoflakes in 50 mL of different initial MB concentrations at pH 7 and 30 min as contact time

Table 6 Effect of interfering ions and dyes on the determination of 100 $\mu\text{g L}^{-1}$ of MB

Ions	Interferent-to-analyte ratio
Li^+ , Na^+ , K^+ , SO_4^{2-} , F^- , Cl^- , CO_3^{2-} , ClO_4^- , CH_3COO^- , Ca^{2+} , Mg^{2+} , NO_3^-	1000:1
Ti^+ , Ag^+	700:1
Al^{3+}	500:1
Ni^{2+} , Cd^{2+} , As^{3+} , Cu^{2+} , Sn^{2+} , Xylenol Orange	200:1
Amaranth, Acid Red 129, Methyl Orange, Pb^{2+}	30:1
Rhodamine 6G, Rhodamine B	15:1

50-mL tube for 30 min. The amount of adsorbed MB at equilibrium (q_e (mg g^{-1})) was calculated using Eq. (2):

$$q_e = (C_0 - C_e) \frac{V}{W} \quad (17)$$

where q_e is the amount of adsorbed MB per gram adsorbent at equilibrium (mg g^{-1}) and C_0 and C_e are the concentrations of the MB before and after adsorption (mg L^{-1}), V and W are the volume of the aqueous phase (L) and the mass of the adsorbent (g), respectively [61]. The removal process by a homogenous identical site surface with negligible interaction is described by the Langmuir equation [10]:

$$\frac{C_e}{q_e} = \frac{1}{K_L Q_m} + \frac{C_e}{Q_m} \quad (18)$$

where C_e is the equilibrium molar concentration of the dye (mg L^{-1}), q_e is the number of moles of solute adsorbed per unit weight at concentration C (mol g^{-1}), Q_m is the maximum adsorption capacity, and K_L is the Langmuir constant or adsorption equilibrium constant (L mg^{-1}) that is related to the apparent energy of sorption [8]. The Langmuir plot (C_e/q_e vs. C_e) for MB adsorption at room temperatures is a straight line, and the values of

Table 7 Analytical characteristics of the proposed method

Analytical parameter	Value
Linear range ($\mu\text{g L}^{-1}$)	2.0–350
Intercept	0.004
Slope	0.0159
Correlation coefficient	0.9996
Detection limit ($\mu\text{g L}^{-1}$)	0.65
Limit of quantification ($\mu\text{g L}^{-1}$)	2.05
Preconcentration factor	100.0
Enrichment factor	120.0
Relative standard deviation (RSD %) ($n = 10$)	1.05 ($20 \mu\text{g L}^{-1}$) 1.65 ($100 \mu\text{g L}^{-1}$)

Table 8 Determination of MB in different water samples

Samples	MB added ($\mu\text{g mL}^{-1}$)	MB found ^a ($\mu\text{g mL}^{-1}$)	Recovery (%)
Domestic wastewater	–	15.54 ± 0.2	–
	10	25.29 ± 0.6	97.50
	20	36.13 ± 0.5	102.95
Beshar water ^b	–	7.89 ± 0.2	–
	10	17.80 ± 0.3	99.10
	20	27.00 ± 0.3	96.00
Karoon water ^c	–	10.33 ± 0.4	–
	10	20.55 ± 0.6	102.20
	20	30.00 ± 0.7	103.35

^a $\bar{x} \pm ts\sqrt{n}$ at 95 % confidence ($n = 5$)

^b A river in a non-industrial city

^c A river in an industrial city

Q_m and K_L constants and the correlation coefficients for this model are presented in Table 5 and Fig. 9.

Reusability of $\text{Cu}(\text{OH})_2$ nanoflakes sorbent

In order to evaluate the reusability of the sorbent, MB– $\text{Cu}(\text{OH})_2$ –nanoflakes were eluted with a mixture of methanol and nitric acid solution and then washed with water. The sorbent was reused several times. Our results showed that each 0.0055 g of the sorbent can be used five times without any significant change in its properties and sorption capacity.

Interferences study

In order to assess the selectivity of the method, the effect of common matrix ions and some dyes which may interfere with the determination of MB was examined under the optimum conditions (Table 6). To carry out an interference study, the absorbance of a constant MB concentration ($100 \mu\text{g L}^{-1}$) was measured before and after adding interfering ions and dyes. A relative error of $\pm 5\%$ in the absorbance measurement was considered as interference. Our results demonstrated that the most common coexisting ions did not show a serious effect on the determination and separation of the MB dye. The two cationic dyes interfered more than the other anionic dyes. This can be attributed to the effect of pH value because the cationic dyes are more extractable than anionic dyes at this pH.

Analytical figures and merit

The analytical characteristic data for the present dispersive CPE–SPE system are shown in Table 7. Under the optimum conditions, a calibration graph was constructed that was linear in the range of 2.0–350.0 $\mu\text{g L}^{-1}$ of MB dye with a

Table 9 Comparison of removal efficiency of Cu(OH)₂ nanoflakes with some previously reported MB adsorption onto various sorbents

Adsorbent	pH	Adsorption capacity (mg/g)	Adsorption dose	Reference
RL-GO ^a	7.0	529.10	0.015 g	[65]
Cotton stalk	7.0	147.06	4.00 g/L	[66]
Powdered activated carbon	7.0	91.0	0.1045 g	[67]
TiO ₂ @yeast	9.0	271.34	0.05 g/L	[68]
Fe ₃ O ₄ @ZIF-8	–	20.20	1.00 g/L	[69]
ACNTs ^b	11	46.21	0.40 g/L	[70]
Cu(OH) ₂ nanoflakes	7.0	122.68	0.0055 g, ca. 0.11 g/L	This work

^a Rhamnolipid-functionalized graphene oxide

^b Amorphous carbon nanotubes

correlation coefficient (R) of 0.9996 indicating its good linearity. The equation of the line for MB was $A = 0.0159C + 0.0040$, where A is the absorbance and C is the concentration of MB in micrograms per liter in the initial solution. The limits of detection ($LOD = 3\sigma_{y/x}/b$) and quantification ($LOQ = 10\sigma_{y/x}/b$) [62] were found to be 0.65 and $2.05 \mu\text{g L}^{-1}$, respectively where $\sigma_{y/x}$ is the standard deviation of y residual and b is the slope of the calibration plot [62]. In addition, the relative standard deviation (RSD) for ten replicates of 20 and $100 \mu\text{g L}^{-1}$ of MB dye was 1.05 and 1.65, respectively. A preconcentration factor ($V_{\text{Aqueous}}/V_{\text{Surfactant-rich phase}}$) of 100.0 was achieved, thereby confirming the sensitivity of the developed dispersive SPE–CPE method. An enrichment factor (EF) of 120.0 was achieved; EF is defined as the ratio the analyte concentration in the sedimented phase to its initial concentration in the sample. The analytical characteristic obtained by the proposed method is better or, at least, comparable to the previously reported methods for removal of MB dye [63, 64].

Application to real samples (scalability)

The developed method was applied to different samples including domestic wastewater, water from Karoon river (located in an industrial city, Ahvaz), and water from Beshar river (Yasouj city) to evaluate the applicability and scalability of the method. Standard additions calibration was utilized to analyze the accuracy of the method (Table 8). Our results confirmed that the developed method provided satisfactory recoveries ranging from 96.00 to 103.35 %. Statistical analysis of these results using Student's t test showed that there is no significant difference between the actual and measured concentrations at the 95 % confidence level.

Role of Cu(OH)₂ nanoflakes

Cu(OH)₂ nanoflakes have two crucial properties that affect the adsorption efficiency: (1) they have a relatively high surface

area and large number of active sites leading to high adsorption capacity and efficiency (adsorption capacity $> 122 \text{ mg g}^{-1}$); (2) they cause very rapid adsorption to the vessel, only by using a very low amount of them (0.0055 g).

Comparison with other adsorbents

The comparison between Cu(OH)₂ nanoflakes and the other sorbents previously studied for the adsorption of MB on the basis of some important analytical parameters, especially maximum adsorption capacity, are given in Table 9. As can be seen in Table 9, the MB adsorption capacity of Cu(OH)₂ nanoflakes at room temperature (ca. 298 K) is 122.68 mg/g , which is comparable to or higher than those reported previously. In addition, by comparison of the amount of adsorbent used in Table 9, it is observed the amount of adsorbent in our study is very negligible (0.0055 g of sorbent, ca. 0.11 g/L) and is better than or comparable to previous studies. The two aforementioned facts prove the efficiency of our method for removal of MB from contaminated water.

Conclusions

This article presents a new efficient method for removal of MB dye in wastewater. The new method developed in this study is based on a combined dispersive solid phase and cloud point extraction using Cu(OH)₂ nanoflakes as sorbent for spectrophotometric determination of MB dye. RSM with CCD was used for the performance evaluation of the parameters affecting the extraction efficiency. The developed method showed remarkable advantages for efficient removal of MB from different wastewater resources including high preconcentration factor, low LOD, very negligible amount of sorbent and solvent, and high accuracy. Unlike most previous studies on SPE–CPE (which used commercial nanoparticles), we successfully synthesized a new efficient sorbent (Cu(OH)₂ nanoflakes) for MB removal.

Compliance with ethical standards There are no known conflicts of interest associated with this publication and there has been no significant financial support for this work that could have influenced its outcome.

References

1. Khajeh M, Kaykhai M, Sharafi A. Application of PSO-artificial neural network and response surface methodology for removal of methylene blue using silver nanoparticles from water samples. *J Ind Eng Chem*. 2013;19(5):1624–30.
2. Feng Y, Zhou H, Liu G, Qiao J, Wang J, Lu H, et al. Methylene blue adsorption onto swede rape straw (*Brassica napus* L.) modified by tartaric acid: equilibrium, kinetic and adsorption mechanisms. *Bioresour Technol*. 2012;125:138–44.
3. Liu Y, Wang J, Zheng Y, Wang A. Adsorption of methylene blue by kapok fiber treated by sodium chlorite optimized with response surface methodology. *Chem Eng J*. 2012;184:248–55.
4. Ghaedi M, Nasab AG, Khodadoust S, Sahraei R, Daneshfar A. Characterization of zinc oxide nanorods loaded on activated carbon as cheap and efficient adsorbent for removal of methylene blue. *J Ind Eng Chem*. 2015;21:986–93.
5. Karimi H, Ghaedi M. Application of artificial neural network and genetic algorithm to modeling and optimization of removal of methylene blue using activated carbon. *J Ind Eng Chem*. 2014;20(4):2471–6.
6. Ghaedi M, Heidarpour S, Kokhdan SN, Sahraie R, Daneshfar A, Brazesh B. Comparison of silver and palladium nanoparticles loaded on activated carbon for efficient removal of methylene blue: kinetic and isotherm study of removal process. *Powder Technol*. 2012;228:18–25.
7. Mahapatra K, Ramteke D, Paliwal L. Production of activated carbon from sludge of food processing industry under controlled pyrolysis and its application for methylene blue removal. *J Anal Appl Pyrol*. 2012;95:79–86.
8. Nekouei F, Kargarzadeh H, Nekouei S, Tyagi I, Agarwal S, Gupta VK. Preparation of nickel hydroxide nanoplates modified activated carbon for malachite green removal from solutions: kinetic, thermodynamic, isotherm and antibacterial studies. *Process Saf Environ*. 2016;102:85–97.
9. Nekouei F, Nekouei S, Tyagi I, Gupta VK. Kinetic, thermodynamic and isotherm studies for acid blue 129 removal from liquids using copper oxide nanoparticle-modified activated carbon as a novel adsorbent. *J Mol Liq*. 2015;201:124–33.
10. Nekouei F, Noorizadeh H, Nekouei S, Asif M, Tyagi I, Agarwal S, et al. Removal of malachite green from aqueous solutions by cuprous iodide–cupric oxide nano-composite loaded on activated carbon as a new sorbent for solid phase extraction: Isotherm, kinetics and thermodynamic studies. *J Mol Liq*. 2016;213:360–8.
11. Nekouei S, Nekouei F, Tyagi I, Agarwal S, Gupta VK. Mixed cloud point/solid phase extraction of lead (II) and cadmium (II) in water samples using modified-ZnO nanopowders. *Process Saf Environ*. 2016;99:175–85.
12. Mahmoodian H, Moradi O, Shariatzadeha B, Salehf TA, Tyagi I, Maity A, et al. Enhanced removal of methyl orange from aqueous solutions by poly HEMA–chitosan–MWCNT nano-composite. *J Mol Liq*. 2015;202:189–98.
13. Nekouei F, Kargarzadeh H, Nekouei S, Keshtpour F, Makhlof ASH. Novel, facile, and fast technique for synthesis of AgCl nanorods loaded on activated carbon for removal of methylene blue dye. *Process Saf Environ*. 2016;103:212–26.
14. Fang R, Cheng X, Xu X. Synthesis of lignin-base cationic flocculant and its application in removing anionic azo-dyes from simulated wastewater. *Bioresour Technol*. 2010;101(19):7323–9.
15. Zheng Y, Yu S, Shuai S, Zhou Q, Cheng Q, Liu M, et al. Color removal and COD reduction of biologically treated textile effluent through submerged filtration using hollow fiber nanofiltration membrane. *Desalination*. 2013;314:89–95.
16. Sun Y, Wang G, Dong Q, Qian B, Meng Y, Qiu J. Electrolysis removal of methyl orange dye from water by electrospun activated carbon fibers modified with carbon nanotubes. *Chem Eng J*. 2014;253:73–7.
17. García-Montaña J, Domenech X, García-Hortal JA, Torrades F, Peral J. The testing of several biological and chemical coupled treatments for Cibacron Red FN-R azo dye removal. *J Hazard Mater*. 2008;154(1):484–90.
18. Khan MAN, Siddique M, Wahid F, Khan R. Removal of reactive blue 19 dye by sono, photo and sonophotocatalytic oxidation using visible light. *Ultrason Sonochem*. 2015;26:370–7.
19. Guo J-Z, Li B, Liu L, Lv K. Removal of methylene blue from aqueous solutions by chemically modified bamboo. *Chemosphere*. 2014;111:225–31.
20. Chem J-M, Huang S-N. Study of nonlinear wave propagation theory. 1. Dye adsorption by activated carbon. *Ind Eng Chem Res*. 1998;37(1):253–7.
21. Özacar M, Şengil IA. Adsorption of reactive dyes on calcined aluminate from aqueous solutions. *J Hazard Mater*. 2003;98(1):211–24.
22. Mousavi R, Nekouei F. Cloud point extraction of toxic reactive black 5 dye from water samples using Triton X-100 as nonionic surfactant. *J Chem*. 2011;8(4):1606–13.
23. Abedi S, Nekouei F. Removal of direct yellow 12 from water samples by cloud point extraction using Triton X-100 as nonionic surfactant. *J Chem*. 2011;8(4):1588–95.
24. Nekouei FNAS. Simultaneous cloud point extraction and ion association system for preconcentration of cadmium (II) in the presence of zwitterionic surfactant 3-[(3-cholamidopropyl)-dimethylammonium]-1-propanesulphonate as a chelating agent prior to its spectrophotometric determination. *Indian J Sci Res*. 2014;8(1):130–7.
25. Nekouei S, Nekouei F. Application of cloud point extraction for the determination of manganese (II) in water samples. *Chiang Mai J Sci*. 2015;42(2):417–28.
26. Nekouei S, Nekouei F. Cloud point extraction and spectrophotometry in the determination of As (III) using amaranth in water samples of rivers located in industrial and non-industrial areas. *Curr Sci India*. (00113891). 2014;107(10).
27. Nekouei S, Nekouei F. Cloud point extraction and spectrophotometric determination of As (III) using brilliant black BN as an extraction agent in water samples. *Studia UBB Chemia*. 2015;60.
28. Nekouei S, Nekouei F, Ulusoy Hİ, Noorizadeh H. Simultaneous application of cloud point and solid-phase extraction for determination of Fe (III) and Cu (II) ions by using SnO₂ nanopowder in micellar medium. *Desalin Water Treat*. 2016;57(27):12653–62.
29. Nazar MF, Shah SS, Eastoe J, Khan AM, Shah A. Separation and recycling of nanoparticles using cloud point extraction with non-ionic surfactant mixtures. *J Colloid Interface Sci*. 2011;363(2):490–6.
30. Tuzen M, Saygi KO, Usta C, Soy lak M. *Pseudomonas aeruginosa* immobilized multiwalled carbon nanotubes as biosorbent for heavy metal ions. *Bioresour Technol*. 2008;99(6):1563–70.
31. Aslan N. Application of response surface methodology and central composite rotatable design for modeling the influence of some operating variables of a multi-gravity separator for coal cleaning. *Fuel*. 2007;86(5):769–76.
32. Kwak J-S. Application of Taguchi and response surface methodologies for geometric error in surface grinding process. *Int J Mach Tool Manuf*. 2005;45(3):327–34.
33. Diniz KM, Tarley CRT. Speciation analysis of chromium in water samples through sequential combination of dispersive magnetic solid phase extraction using mesoporous amino-functionalized

- Fe₃O₄/SiO₂ nanoparticles and cloud point extraction. *Microchem J.* 2015;123:185–95.
34. Pourreza N, Naghdi T. Combined cloud point-solid phase extraction by dispersion of TiO₂ nanoparticles in micellar media followed by semi-microvolume UV–vis spectrophotometric detection of zinc. *Talanta.* 2014;128:164–9.
 35. Giokas DL, Zhu Q, Pan Q, Chisvert A. Cloud point–dispersive μ -solid phase extraction of hydrophobic organic compounds onto highly hydrophobic core–shell Fe₂O₃@C magnetic nanoparticles. *J Chromatogr A.* 2012;1251:33–9.
 36. Gao N, Wu H, Chang Y, Guo X, Zhang L, Du L, et al. Mixed micelle cloud point-magnetic dispersive μ -solid phase extraction of doxazosin and alfuzosin. *Spectrochim Acta A.* 2015;134:10–6.
 37. Harish K, Renu R, Kumar SR. Synthesis of nickel hydroxide nanoparticles by reverse micelle method and its antimicrobial activity. *Res J Chem Sci.* ISSN. 2011;2231:606X.
 38. Im J-K, Cho I-H, Kim S-K, Zoh K-D. Optimization of carbamazepine removal in O₃/UV/H₂O₂ system using a response surface methodology with central composite design. *Desalination.* 2012;285:306–14.
 39. Asfaram A, Ghaedi M, Agarwal S, Tyagi I, Gupta VK. Removal of basic dye Auramine-O by ZnS: Cu nanoparticles loaded on activated carbon: optimization of parameters using response surface methodology with central composite design. *RSC Adv.* 2015;5(24):18438–50.
 40. Khataee A, Zarei M, Fathinia M, Jafari MK. Photocatalytic degradation of an anthraquinone dye on immobilized TiO₂ nanoparticles in a rectangular reactor: destruction pathway and response surface approach. *Desalination.* 2011;268(1):126–33.
 41. Sartale S, Sankapal B, Lux-Steiner M, Ennaoui A. Preparation of nanocrystalline ZnS by a new chemical bath deposition route. *Thin Solid Films.* 2005;480:168–72.
 42. Wang Y, Jiang T, Meng D, Kong J, Jia H, Yu M. Controllable fabrication of nanostructured copper compound on a Cu substrate by a one-step route. *RSC Adv.* 2015;5(21):16277–83.
 43. Duran A, Tuzen M, Soylak M. Preconcentration of some trace elements via using multiwalled carbon nanotubes as solid phase extraction adsorbent. *J Hazard Mater.* 2009;169(1):466–71.
 44. Devamani RHP, Alagar M. Synthesis and characterisation of copper II hydroxide nano particles. *Nano Biomed Eng.* 2013;5(3).
 45. Linkov P, Artemyev M, Efimov AE, Nabiev I. Comparative advantages and limitations of the basic metrology methods applied to the characterization of nanomaterials. *Nanoscale.* 2013;5(19):8781–98.
 46. Singh DP, Ojha AK, Srivastava ON. Synthesis of different Cu(OH)₂ and CuO (nanowires, rectangles, seed-, belt-, and sheetlike) nanostructures by simple wet chemical route. *J Phys Chem C.* 2009;113(9):3409–18.
 47. Pramanik A, Maiti S, Mahanty S. Metal hydroxides as a conversion electrode for lithium-ion batteries: a case study with a Cu(OH)₂ nanoflower array. *J Mater Chem A.* 2014;2(43):18515–22.
 48. Zhang L, Lu W, Feng Y, Ni J, Lü Y, Shang X. Facile synthesis of leaf-like Cu(OH)₂ and its conversion into CuO with nanopores. *Acta Phys-Chim Sin.* 2008;24(12):2257–62.
 49. Yang Y, Fan X, Casillas G, Peng Z, Ruan G, Wang G, et al. Three-dimensional nanoporous Fe₂O₃/Fe₃C-graphene heterogeneous thin films for lithium-ion batteries. *ACS Nano.* 2014;8(4):3939–46.
 50. Armand M, Tarascon J-M. Building better batteries. *Nature.* 2008;451(7179):652–7.
 51. Rahman QI, Ahmad M, Misra SK, Lohani MB. Hexagonal ZnO nanorods assembled flowers for photocatalytic dye degradation: growth, structural and optical properties. *Superlattice Microst.* 2013;64:495–506.
 52. Sahu MK, Sahu UK, Patel RK. Adsorption of safranin-O dye on CO₂ neutralized activated red mud waste: process modelling, analysis and optimization using statistical design. *RSC Adv.* 2015;5(53):42294–304.
 53. Yi S, Su Y, Qi B, Su Z, Wan Y. Application of response surface methodology and central composite rotatable design in optimizing the preparation conditions of vinyltriethoxysilane modified silicalite/polydimethylsiloxane hybrid pervaporation membranes. *Sep Purif Technol.* 2010;71(2):252–62.
 54. Su S-N, Nie H-L, Zhu L-M, Chen T-X. Optimization of adsorption conditions of papain on dye affinity membrane using response surface methodology. *Bioresour Technol.* 2009;100(8):2336–40.
 55. Evans M. Optimisation of manufacturing processes: a response surface approach. London: Maney; 2003.
 56. Fan J, Yi C, Lan X, Yang B. Optimization of synthetic strategy of 4'-(5"-di-tert-butyl)benzo-18-crown-6 using response surface methodology. *Org Process Res Dev.* 2013;17(3):368–74.
 57. Gürkan R, Aksoy Ü, Ulusoy Hİ, Akçay M. Determination of low levels of molybdenum (VI) in food samples and beverages by cloud point extraction coupled with flame atomic absorption spectrometry. *J Food Compos Anal.* 2013;32(1):74–82.
 58. Arain SS, Kazi TG, Arain JB, Afridi HI, Brahman KD. Preconcentration of toxic elements in artificial saliva extract of different smokeless tobacco products by dual-cloud point extraction. *Microchem J.* 2014;112:42–9.
 59. Sato N, Mori M, Itabashi H. Cloud point extraction of Cu (II) using a mixture of triton X-100 and dithizone with a salting-out effect and its application to visual determination. *Talanta.* 2013;117:376–81.
 60. Gouda AA. Solid-phase extraction using multiwalled carbon nanotubes and quinalizarin for preconcentration and determination of trace amounts of some heavy metals in food, water and environmental samples. *Int J Environ Anal Chem.* 2014;94(12):1210–22.
 61. Omri A, Benzina M. Removal of manganese (II) ions from aqueous solutions by adsorption on activated carbon derived a new precursor: Ziziphus spina-christi seeds. *Alex Eng J.* 2012;51(4):343–50.
 62. El-Shahawi M, Hamza A, Al-Sibaai A, Bashammakh A, Al-Saidi H. A new method for analysis of sunset yellow in food samples based on cloud point extraction prior to spectrophotometric determination. *J Ind Eng Chem.* 2013;19(2):529–35.
 63. Razmara RS, Daneshfar A, Sahrai R. Determination of methylene blue and sunset yellow in wastewater and food samples using salting-out assisted liquid–liquid extraction. *J Ind Eng Chem.* 2011;17(3):533–6.
 64. Xu JZ, Dai L, Wu B, Ding T, Zhu JJ, Lin H, et al. Determination of methylene blue residues in aquatic products by liquid chromatography-tandem mass spectrometry. *J Sep Sci.* 2009;32(23-24):4193–9.
 65. Wu Z, Zhong H, Yuan X, Wang H, Wang L, Chen X, et al. Adsorptive removal of methylene blue by rhamnolipid-functionalized graphene oxide from wastewater. *Water Res.* 2014;67:330–44.
 66. Deng H, Lu J, Li G, Zhang G, Wang X. Adsorption of methylene blue on adsorbent materials produced from cotton stalk. *Chem Eng J.* 2011;172(1):326–34.
 67. Yener J, Kopac T, Dogu G, Dogu T. Dynamic analysis of sorption of methylene blue dye on granular and powdered activated carbon. *Chem Eng J.* 2008;144(3):400–6.
 68. Chen L, Bai B. Equilibrium, kinetic, thermodynamic, and in situ regeneration studies about methylene blue adsorption by the raspberry-like TiO₂@ yeast microspheres. *Ind Eng Chem Res.* 2013;52(44):15568–77.
 69. Zheng J, Cheng C, Fang W-J, Chen C, Yan R-W, Huai H-X, et al. Surfactant-free synthesis of a Fe₃O₄@ZIF-8 core–shell heterostructure for adsorption of methylene blue. *CrystEngComm.* 2014;16(19):3960–4.
 70. Zhang Y-X, Liu Z-L, Sun B, Xu W-H, Liu J-H. An alternative hydrothermal route to amorphous carbon nanotubes for treatment of organic pollutants in water. *RSC Adv.* 2013;3(45):23197–206.